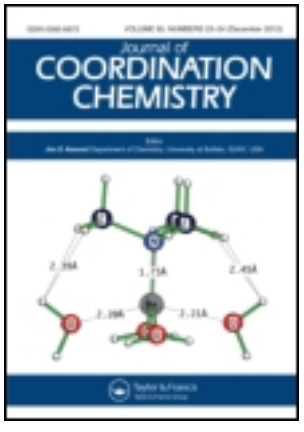

Journal of Coordination Chemistry
Publication details, including instructions for authors and subscription information:
http://www.tandfonline.com/loi/gcoo20

π-π Stacking, hydrogen bonding and anti-ferromagnetic coupling mechanism on a mononuclear Cu(II) complex

Hong Li [a] , Shi-Guo Zhang [a] , Long-Miao Xie [b] , Li Yu [b] & Jing-Min Shi [b]

[a] Department of Chemistry and Chemical Engineering , Institute of Material Chemistry, Binzhou University , Binzhou 256603 , P.R. China

[b] Department of Chemistry , Shandong Normal University , Jinan 250014 , P.R. China

Published online: 14 Apr 2011.

To cite this article: Hong Li , Shi-Guo Zhang , Long-Miao Xie , Li Yu & Jing-Min Shi (2011) π-π Stacking, hydrogen bonding and anti-ferromagnetic coupling mechanism on a mononuclear Cu(II) complex, Journal of Coordination Chemistry, 64:8, 1456-1468, DOI: 10.1080/00958972.2011.572968

To link to this article: http://dx.doi.org/10.1080/00958972.2011.572968

Journal of Coordination Chemistry
Vol. 64, No. 8, 20 April 2011, 1456–1468

π–π Stacking, hydrogen bonding and anti-ferromagnetic coupling mechanism on a mononuclear Cu(II) complex

HONG LI†, SHI-GUO ZHANG†, LONG-MIAO XIE‡,
LI YU‡ and JING-MIN SHI*‡

†Department of Chemistry and Chemical Engineering,
Institute of Material Chemistry, Binzhou University, Binzhou 256603, P.R. China
‡Department of Chemistry, Shandong Normal University,
Jinan 250014, P.R. China

(*Received 19 January 2011; in final form 4 March 2011*)

Weak anti-ferromagnetic coupling is observed in a mononuclear copper(II) complex, $[Cu(Pid)(OSO_3)(H_2O)]\cdot(H_2O)$ (Pid = 2,2′-(1,10-phenanthrolin-2-ylimino)diethanol). The Cu(II) complex is a distorted square pyramid. Analysis of the crystal structure indicates that there are two types of magnetic coupling pathways, where one pathway involves π–π stacking between adjacent complexes and the second one involves the O–H···O hydrogen bonds between adjacent complexes. The variable-temperature magnetic susceptibilities show that there is a weak anti-ferromagnetic coupling between adjacent Cu(II) ions with Curie–Weiss constant $\theta = -13.71\,K = -9.93\,cm^{-1}$. Theoretical calculations reveal that the π–π stacking resulted in anti-ferromagnetic coupling with $2J = -6.30\,cm^{-1}$, and the O–H···O hydrogen-bonding pathway led to a weaker anti-ferromagnetic interaction with $2J = -3.38\,cm^{-1}$. The theoretical calculations also indicate that anti-ferromagnetic coupling sign from the π–π stacking accords with the McConnell I spin-polarization mechanism.

Keywords: Crystal structure; Magnetic coupling; π–π Stacking; Hydrogen bond; Copper complex

1. Introduction

Major advances in molecular magnetism have been made in both their description and their application as new molecular-based materials [1–3]. In the reported molecular magnetic compounds, the majority of spin-carriers, such as metallic ions and radicals, deal with systems where the coupling spin-carriers are connected by bridging ligands [4–8]; the magnetic interactions are through bond exchange. As intermolecular forces, π–π stacking interaction and hydrogen bonding have also played a role in magnetic interaction. Some authors attributed the strong ferromagnetic order to π–π stacking interaction [4], and other authors found that π–π stacking led to a strong anti-ferromagnetic interaction between spin-carriers [9–11]. Another paper [12] reported strong anti-ferromagnetic coupling between Cu(II) ions through O–H···O hydrogen

*Corresponding author. Email: shijingmin1955@gmail.com

Journal of Coordination Chemistry
ISSN 0095-8972 print/ISSN 1029-0389 online © 2011 Taylor & Francis
DOI: 10.1080/00958972.2011.572968

bonds. Intermolecular force should be a key factor in magnetic coupling properties, but papers dealing with magnetic exchange interaction through intermolecular forces, such as hydrogen bonding [13–20], π–π stacking [9–11], and X–H $\cdots$ π interaction [16], are scarce, mostly dealing with radicals [13, 20] or complexes [11, 21–23] with radicals as ligands. Although the magnetic coupling signs of some compounds have been explained using the McConnell I spin-polarization mechanism and the McConnell II charge transfer mechanism, there are still points to be resolved. In addition, the factors that dominate magnetic coupling mechanism have not been mentioned by them. Therefore, it is important to design and synthesize complexes dealing with π–π stacking interaction and hydrogen bonding and study their magnetic coupling mechanism.

Derivatives of 1,10-phenanthroline are ideal ligands that possess both a strong chelated coordination group and a larger conjugation plane which may be useful to form complexes with π–π stacking and relevant magnetic coupling pathways. Ideally, 2,2′-(1,10-Phenanthrolin-2-ylimino)diethanol as a derivative of 1,10-phenanthroline should be tridentate or tetradentate, but only a mononuclear Cd(II) complex [24] has been reported and there is no paper that correlates magnetism with its π–π stacking and hydrogen bonding. We synthesized the Cu(II) complex with 2,2′-(1,10-phenanthrolin-2-ylimino)diethanol and report its magnetic coupling mechanism from π–π stacking and hydrogen-bonding pathways, both involving the experimental and theoretical calculations.

2. Experimental

2.1. *Materials*

In this study, 2,2′-(1,10-Phenanthrolin-2-ylimino)diethanol was synthesized by the reaction of 2-chloro-1,10-phenanthroline and diethanolamine. All other chemicals are of analytical grade and used without purification.

2.2. *Preparation of [Cu(Pid)(OSO$_3$)(H$_2$O)]·(H$_2$O)*

In this study, 10 mL H_2O solution of $CuSO_4 \cdot 5H_2O$ (0.0367 g, 0.147 mmol) was added to 10 mL of methanol solution containing 2,2′-(1,10-phenanthrolin-2-ylimino)diethanol (0.0486 g, 0.171 mmol) and the mixed solution was stirred for a few minutes. Blue single crystals were obtained after the filtrate was allowed to slowly evaporate at room temperature for a week. IR (cm^{-1}): 3425(s), 1628(m), 1596(w), 1572(w), 1532(m), 1491(w), 1111(s), and 1079(s). Anal. Calcd (%) for $C_{16}H_{21}CuN_3O_8S$: (Fw 478.96) C, 40.12; H, 4.42; N, 8.78; and Cu, 13.27. Found (%): C, 40.31; H, 4.71; N, 9.13; and Cu, 13.73.

2.3. *Physical measurements*

Infrared spectra were recorded with a Bruker Tensor 27 infrared spectrometer in the 4000–500 cm^{-1} region using KBr disks. C, H, and N elemental analyses were carried out on a Perkin-Elmer 240 instrument. Variable-temperature magnetic susceptibilities of microcrystalline powder sample were measured in a magnetic field 1 K Oe from 2 to

300 K on a SQUID magnetometer. The data were corrected for magnetization of the sample holder and for diamagnetic contributions of the complex which were estimated from Pascal's constants.

2.4. *Computational details*

The magnetic interactions between Cu(II) ions were studied on the basis of density functional theory (DFT) coupled with the broken-symmetry approach (BS) [25–27]. The exchange coupling constants J have been evaluated by calculating the energy difference between the high-spin state (E_{HS}) and the broken symmetry state (E_{BS}). Assuming the spin Hamiltonian is defined as,

$$\hat{H} = -2J\hat{S}_1 \cdot \hat{S}_2 \tag{1}$$

if the spin-projected approach is used, the equation proposed by Noodleman [25–27] to extract the J value for a binuclear transition–metal complex is

$$J = \frac{E_{BS} - E_{HS}}{4S_1S_2} \tag{2}$$

To obtain exchange coupling constants J, Orca 2.8.0 calculations [28] were performed with the popular spin-unrestricted hybrid functional B3LYP proposed by Becke [29, 30] and Lee *et al*. [31], which can provide J values in agreement with the experimental data for transition–metal complexes [32, 33]. Tri-ζ basis sets with one polarization function def2-TZVP [34, 35] basis set proposed by Ahlrichs and co-workers for all atoms was used in our calculations. Strong convergence criteria were used in order to ensure that the results are well converged with respect to technical parameters (the system energy was set to be smaller than 10^{-7} Hartree).

2.5. *X-ray crystallographic analysis of the complex*

A blue single crystal of dimensions $0.51 \times 0.04 \times 0.03\,\text{mm}^3$ was selected and subsequently glued to the tip of a glass fiber. The determination of the crystal structure at 25°C was carried out on an X-ray diffractometer (Bruker Smart-1000 CCD) using graphite monochromated Mo-Kα radiation ($\lambda = 0.71073$ Å). Corrections for L_p factors were applied and all non-hydrogen atoms were refined with anisotropic thermal parameters. Hydrogens from hydroxyl and H_2O were located in a difference Fourier map and other hydrogens were placed in calculated positions; all hydrogens were refined as riding. The programs used for structure solution and refinement were SHELXS-97 and SHELXL-97, respectively. The pertinent crystallographic data and structural refinement parameters are summarized in table 1.

3. Results and discussion

3.1. *Crystal structure of [Cu(Pid)(OSO_3)(H_2O)]·(H_2O)*

Figure 1 shows the coordination diagram with the atom numbering scheme. Table 2 gives the coordination bond lengths and the associated angles. Coordination bonds

Table 1. Crystal data and structure refinements for the complex.

Empirical formula	$C_{16}H_{21}CuN_3O_8S$
Formula weight, Mr	478.96
Crystal system	Monoclinic
Space group	$P2_1/n$
Unit cell dimensions (Å, °)	
a	15.589(4)
b	7.2191(16)
c	16.476(4)
β	100.437(3)
Volume (Å^3), Z	1823.6(7), 4
Calculated density (g cm^{-1})	1.745
Absorption coefficient, μ (mm^{-1})	1.366
Reflections collected	10187
Independent reflections	3912 [R(int) = 0.060]
Goodness-of-fit on F^2	1.046
Final R indices [$I > 2\sigma(I)$]	$R_1 = 0.0623$, $wR_2 = 0.1309$
Largest difference peak and hole $(\Delta\rho)_{max,mean}$ and $\Delta\rho_{min}$ (e Å^{-3})	0.530 and −0.379

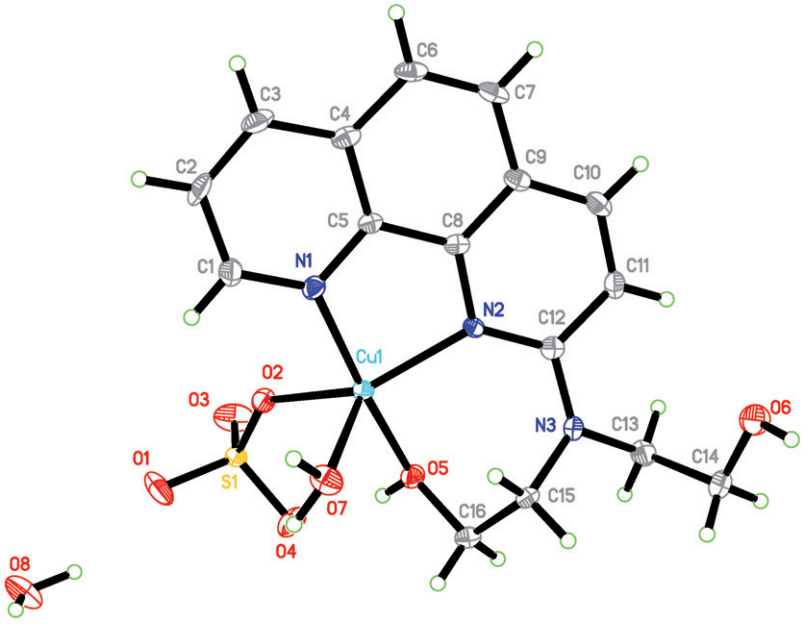

Figure 1. The asymmetric unit and coordination diagram of the complex with atom numbering scheme.

Table 2. Selected bond lengths (Å) and angles (°) for the complex.

Cu1–O5	1.947(3)	Cu1–N1	1.959(3)	Cu1–O2	2.022(3)
Cu1–N2	2.056(3)	Cu1–O7	2.174(3)		
O5–Cu1–N1	171.06(15)	O5–Cu1–O2	88.87(14)	N1–Cu1–O2	88.85(13)
O5–Cu1–N2	94.68(14)	N1–Cu1–N2	82.54(13)	O2–Cu1–N2	146.59(14)
O5–Cu1–O7	92.60(13)	N1–Cu1–O7	96.30(14)	O2–Cu1–O7	99.07(13)
N2–Cu1–O7	113.90(13)				

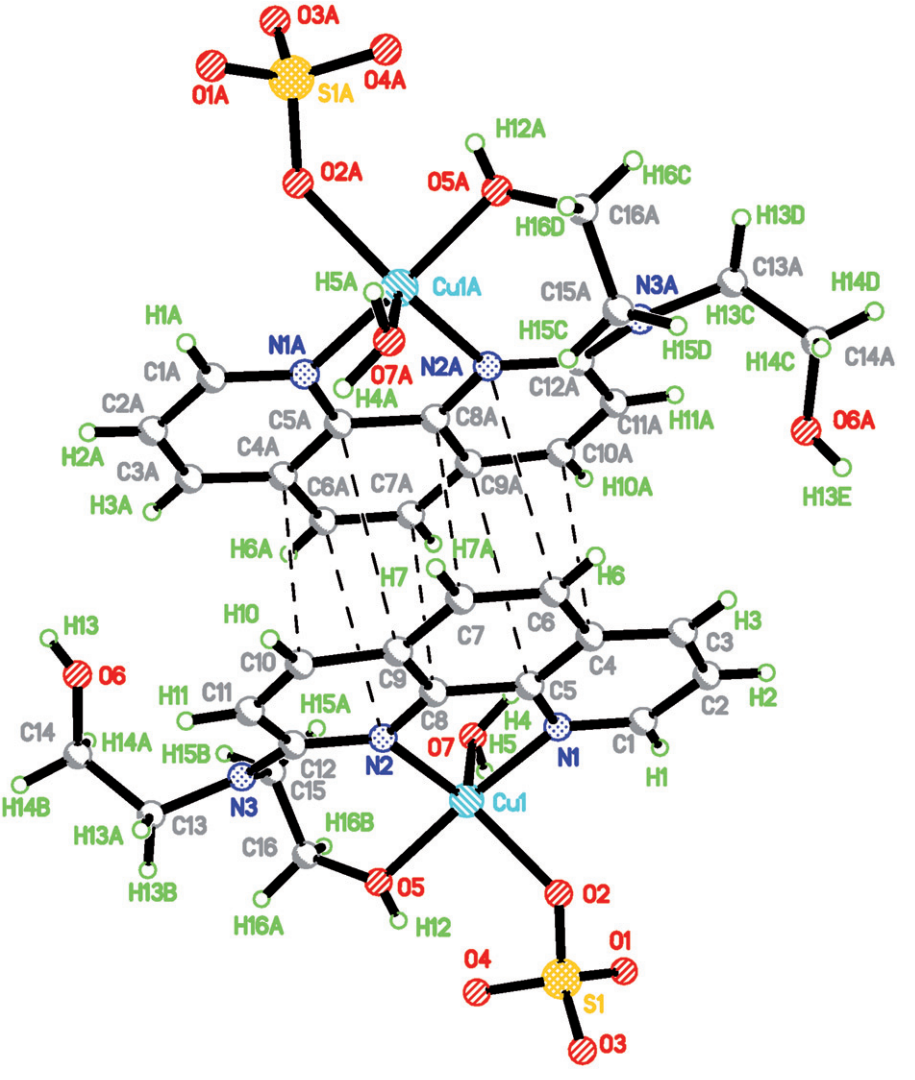

Figure 2. The π–π stacking between adjacent mononuclear Cu(II) complexes (symmetry codes: $1-x$, $-y$, $-z$).

lengths range from 1.947(3)to 2.174(3) Å and the associated angles change from 82.54(13)° to 171.06(15)°. Cu(II) assumes a strongly distorted square pyramidal geometry due to its Addison constant [36] $\tau = (\beta - \alpha)/60 = 0.41$. The non-hydrogen atoms of the 1,10-phenanthroline ring define an approximate plane within 0.0293 Å with a maximum deviation of −0.0608 (34) Å for C12. In the crystal, there is π–π stacking among the adjacent complexes, as shown in figure 2, involving symmetry-related 1,10-phenanthroline rings slipped π-stacking with the relevant distances (3.7 Å as a π–π stacking maximum distance [37]) being C10 · · · C4A (C10A · · · C4), 3.478(7) Å; C7 · · · C8A (C7A · · · C8) 3.413(7) Å; C6 · · · N2A (C6A · · · N2), 3.499(6) Å; C9 · · · C5A (C9A · · · C5), 3.546(6) Å. In addition to the π–π stacking, there are hydrogen bonds

Table 3. Hydrogen bonds lengths (Å) and associated angles (°).

D–H···A	H···A	D···A	∠D–H···A
O7–H4···O3^{i}	1.92	2.817(5)	175
O7–H5···O8A	1.92	2.782(5)	163
O8–H8···O1	1.98	2.817(5)	156
O8–H9···O4^{ii}	2.19	3.027(6)	155
O5–H12···O4	1.80(5)	2.516(5)	162(6)
O6–H13···O1^{iii}	2.06(7)	2.821(6)	160(6)

(i: $x, -1+y, z$), (A: $1-x, 1-y, 1-z$), (ii: $1-x, 1-y, 1-z$), (iii: $-1/2+x, 1/2-y, -1/2+z$).

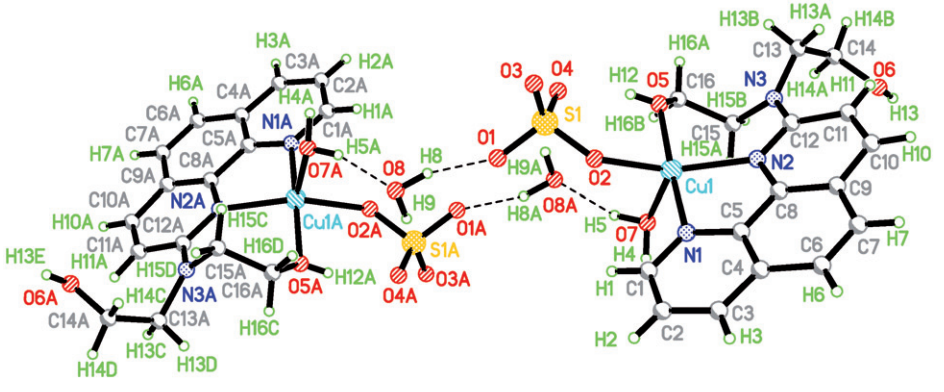

Figure 3. The hydrogen bonding between adjacent mononuclear Cu(II) complexes (symmetry codes: $1-x$, $1-y$, $1-z$).

between adjacent complexes and the adjacent complex and uncoordinated water; relevant hydrogen bond data are listed in table 3. Figure 3 displays two types of the hydrogen bonds, which involve the uncoordinated water and two complexes with Cu1···Cu1A separation of 10.195 Å.

3.2. *Magnetic studies*

3.2.1. Experimental results. The experimental variable-temperature (2 – 300 K) magnetic susceptibilities of the crystal are shown in figure 4, where χ_M is the molar magnetic susceptibility per mononuclear Cu(II) unit and μ_{eff} the magnetic moment per mononuclear Cu(II). Figure 4 shows that χ_M increases with decreasing temperature, reaching a maximum at 2.00 K. The μ_{eff} value at 300 K is 2.07 B.M., larger than the value of isolated per Cu(II) ion (1.73 B.M. for $g_{av}=2$) at room temperature, and the μ_{eff} value decreases with lowering temperature reaching 1.60 B.M. at 2 K, which indicates anti-ferromagnetic coupling among adjacent complexes. The fitting for the experimental data with Curie–Weiss formula, as shown in figure 5, gave the following parameters, $g=2.34$, $\theta=-13.71\,\text{K}=-9.93\,\text{cm}^{-1}$, which further reveals the anti-ferromagnetic interaction among adjacent Cu(II) ions. Because there are π–π stacking and hydrogen-bond interactions among adjacent complexes, we perform theoretical

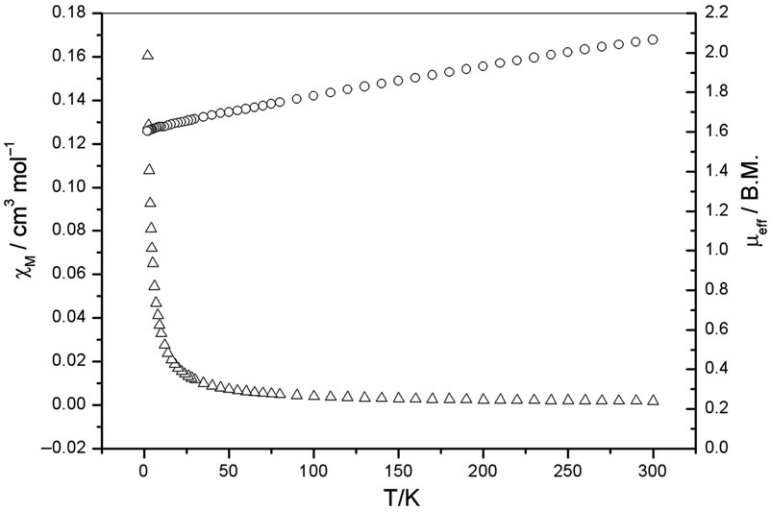

Figure 4. Plots of χ_M (the open triangle for the experimental data) and μ_{eff} (the open circle for the experimental data) *vs.* *T*.

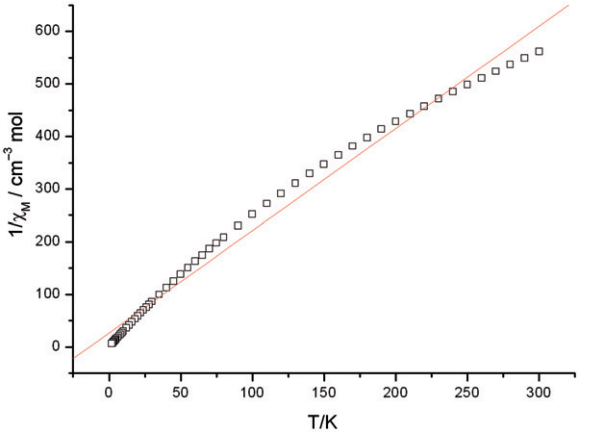

Figure 5. Thermal variation of the reciprocal susceptibility (open square for experimental data).

calculations to understand the coupling mechanisms of the magnetic coupling pathways.

3.2.2. Theoretical study on magnetic interaction. Density function calculations were based on Models 1–4. Model 1 stands for the magnetic coupling pathway of the π–π stacking as shown in figure 2, whereas Model 2 stands for the magnetic coupling pathway of the hydrogen bonding as shown in figure 3. Models 3 and 4 are basically identical with Model 2, but one uncoordinated H_2O is deleted in Model 3 as shown in figure 6, whereas two uncoordinated H_2O molecules are deleted in Model 4, as shown in figure 7. From Models 2 to 4, we may understand the magnetic coupling role of the

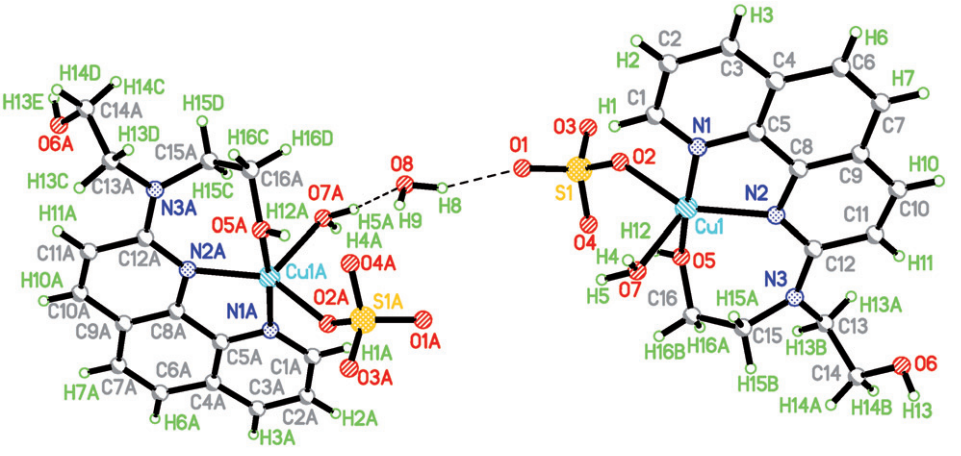

Figure 6. Model 3 for the hydrogen-bonding system deleting one H_2O.

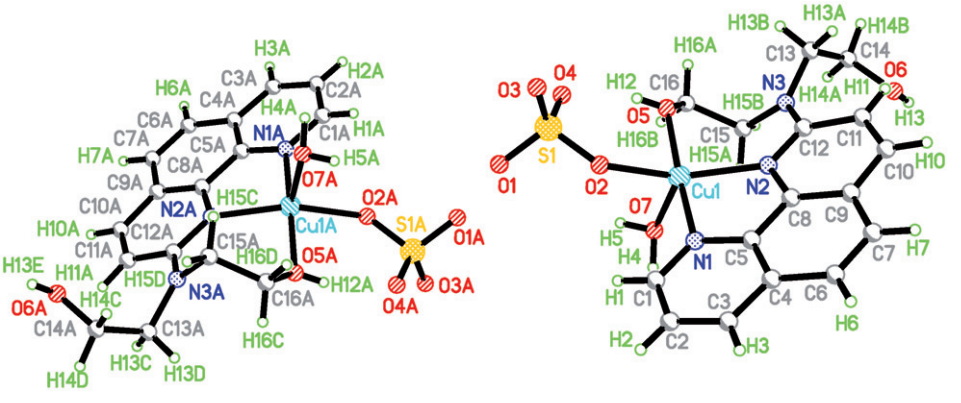

Figure 7. Model 4 for the hydrogen-bonding system deleting two H_2O molecules.

hydrogen bonds. The calculations were constrained by the bond-length data, the associated angles and the relevant locations of complexes and uncoordinated H_2O from the X-ray structure. The calculations gave $2J = -6.30\,cm^{-1}$ for Model 1 and $2J = -3.38\,cm^{-1}$ for Model 2 according to equation (2), which means that both the π–π stacking and the hydrogen bonding are anti-ferromagnetic, but the magnetic coupling magnitude from the π–π stacking pathway is stronger than that of the hydrogen bonds. In addition, the magnetic coupling sign from the experiment is identical with those of the calculations.

The calculations also gave $2J = -20.06\,cm^{-1}$ for Model 3 and $2J = -23.20\,cm^{-1}$ for Model 4, implying that the hydrogen bonds from H_2O molecules resulted in the decrease of the magnetic coupling magnitude of adjacent complexes; it may also indicate that the magnetic interaction does not result from dipole interactions. The literature [15, 17–19, 38–42] reports that hydrogen bonds provide strong magnetic interaction of adjacent complexes, whereas the present hydrogen bonds decrease

Table 4. Calculated atomic spin population of the ground state for Model 1.

Atom	Spin density	Atom	Spin density
C1	−0.007336	C1A	0.007298
C2	0.005241	C2A	−0.005197
C3	−0.004845	C3A	0.004811
C4	0.003410	C4A	−0.003249
C5	−0.001057	C5A	0.001429
C6	−0.000183	C6A	0.000221
C7	0.000581	C7A	−0.000736
C8	−0.000410	C8A	0.000008
C9	0.000566	C9A	−0.000434
C10	−0.001730	C10A	0.001687
C11	0.002177	C11A	−0.002175
C12	−0.002695	C12A	0.002691
C13	−0.000009	C13A	0.000007
C14	−0.000048	C14A	0.000047
C15	0.000658	C15A	−0.000653
C16	−0.001090	C16A	0.001084
Cu1	0.484040	Cu1A	−0.484037
N1	0.064043	N1A	−0.064082
N2	0.044614	N2A	−0.044578
N3	−0.000514	N3A	0.000514
O1	0.096185	O1A	−0.096187
O2	0.162493	O2A	−0.162493
O3	0.071059	O3A	−0.071059
O4	0.079719	O4A	−0.079719
O5	0.044236	O5A	−0.044235
O6	0.000008	O6A	−0.000008
O7	0.000880	O7A	−0.000880
S1	−0.038997	S1A	0.038998

the magnetic coupling magnitude. The difference may be from the different hydrogen-bonding structures. In the present hydrogen-bonding system, H_2O molecules do not take part in coordination, whereas in the reported hydrogen-bonding system [15, 17–19, 38–42], one or two non-hydrogens of the hydrogen-bonding system take part in coordination.

For magnetic coupling, the sign of the π–π stacking McConnell I spin-polarization mechanism [43] has been used to explain the ferromagnetic interaction of $[Mn(Cp^*)2]^+$ $[Ni(dmit)2]^-$ [44]. The McConnell I spin-polarization mechanism considers that a global ferromagnetic coupling arises from interaction between spin densities of opposite sign being predominant, whereas an anti-ferromagnetic coupling results from dominant interaction between spin densities of the same sign. Table 4 or figure 8 shows the spin density population of the ground state of Model 1, and from table 4, we see that the absolute value of the spin density population of each Cu(II) is smaller than 1 and the coordinated N and O exhibit the same sign as Cu(II), suggesting spin delocalization from the two Cu(II) 3d orbitals to the coordinated atoms, whereas opposite spin densities appear on atoms of identical ligands, indicating that spin polarization also exists in this system. Both the spin delocalization and spin polarization may benefit the magnetic coupling through the π–π stacking pathway. In π–π stacking, all pairs of atoms [C10(β)$\cdots$C4A(β), C10A(α)$\cdots$C4(α), C7(α)$\cdots$C8A(α), C7A(β)$\cdots$C8(β), C6(β)$\cdots$N2A(β), C6A(α)$\cdots$N2(α), C9(α)$\cdots$C5A(α) and C9A(β)$\cdots$C5(β)] exhibit the same spin density interaction, and obviously, the

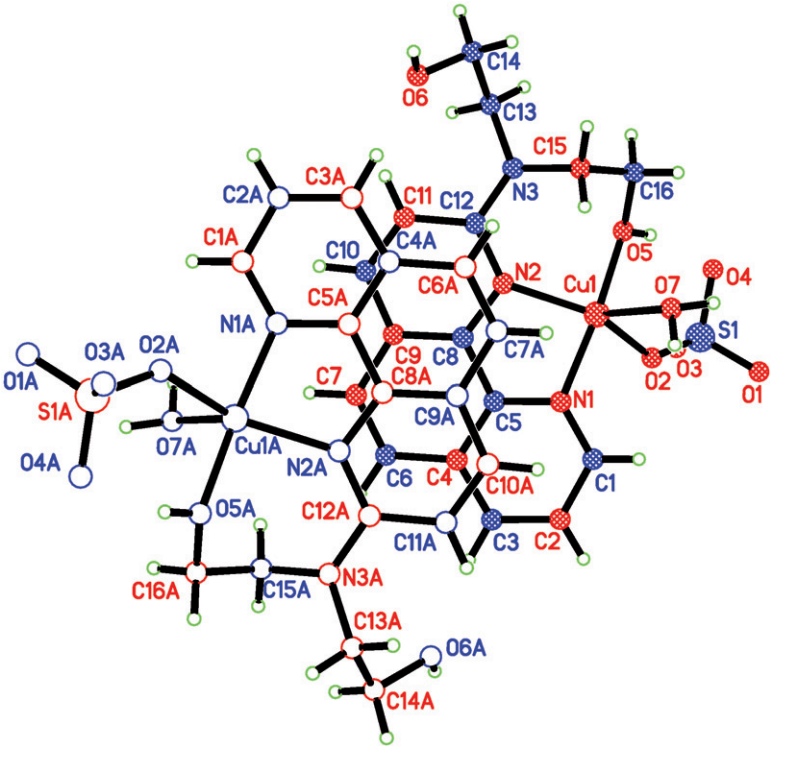

Figure 8. The calculated spin density sign, in which atoms with positive spin density are drawn in red and atoms with negative spin density are drawn in blue.

McConnell I spin-polarization mechanism explains the anti-ferromagnetic coupling mechanism of Model 1.

The calculations also gave the spin density population of the ground state for Model 2, as given in table 5. From table 5, we see that spin delocalization and the spin polarization occur in Model 2, identical with Model 1. Comparing table 5 with table 4, we see that the spin density on Cu(II) of Model 1 is smaller than that of Model 2, implying that the spin delocalization magnitude of Model 1 is stronger than that of Model 2. According to the spin delocalization mechanism [45], the more spin delocalization, the stronger anti-ferromagnetic magnetic coupling magnitude. Hence, the anti-ferromagnetic coupling magnitude in Model 1 should be stronger than that of Model 2, which accords with the magnetic coupling parameters from the calculations.

4. Conclusions

A new Cu(II) complex with 2,2′-(1,10-phenanthrolin-2-ylimino)diethanol as ligand has been synthesized. Its crystal structure shows π–π stacking and O–H$\cdots$O hydrogen bonds between adjacent complexes. The experimental fitting for variable-temperature magnetic susceptibility data with the Curie–Weiss formula reveals a weak anti-ferromagnetic coupling between adjacent Cu(II) complexes. The theoretical calculations

Table 5. Calculated atomic spin population of the ground state for Model 2.

Atom	Spin density	Atom	Spin density
C1	−0.007889	C1A	0.007889
C2	0.005956	C2A	−0.005963
C3	−0.004667	C3A	0.004674
C4	0.003795	C4A	−0.003857
C5	−0.001169	C5A	0.00118
C6	0.000227	C6A	−0.000161
C7	0.000699	C7A	−0.000764
C8	−0.001917	C8A	0.001913
C9	0.000909	C9A	−0.000868
C10	−0.002255	C10A	0.00223
C11	0.002816	C11A	−0.002794
C12	−0.002282	C12A	0.002284
C13	−0.000042	C13A	0.000042
C14	−0.000028	C14A	0.000028
C15	0.000869	C15A	−0.000874
C16	0.000022	C16A	−0.000020
Cu1	0.5787	Cu1A	−0.578698
N1	0.080082	N1A	−0.080088
N2	0.054201	N2A	−0.054202
N3	−0.000436	N3A	0.000437
O1	0.022896	O1A	−0.022896
O2	0.144707	O2A	−0.144707
O3	0.053656	O3A	−0.053656
O4	0.036016	O4A	−0.036015
O5	0.050415	O5A	−0.050415
O6	0.000006	O6A	−0.000006
O7	0.00134	O7A	−0.001340
O8	0.000165	O8A	−0.000165
S1	−0.019639	S1A	0.019639

further reveal that both π–π stacking magnetic exchange pathway and the O–H$\cdots$O hydrogen bonding magnetic exchange pathway exhibit anti-ferromagnetic coupling and the magnetic coupling magnitude from the π–π stacking pathway is larger than that of the O–H$\cdots$O hydrogen-bonding pathway. The magnetic coupling sign of the π–π stacking is explained with a McConnell I spin-polarization mechanism.

Supplementary material

CCDC 801088 contains detailed information of the Crystallographic data for this article, and these data can be obtained free of charge from the Cambridge Crystallographic Data Centre via http://www.ccdc.cam.ac.uk/data_request/cif.

Acknowledgments

This study was supported by the Natural Science Foundation of China (Grant no. 20971080) and the Natural Science Foundation of Shandong Province (Grant no. ZR2009BM026 and ZR2009BL002).

References

[1] J.R. Friedman, M.P. Sarachik, J. Tejada, R. Ziolo. *Phys. Rev. Lett*., **76**, 3830 (1996).
[2] G.L.J.A. Rickken, E. Raupack. *Nature*, **405**, 932 (2000).
[3] S. Tanase, J. Reedijk. *Coord. Chem. Rev*., **250**, 2501 (2006).
[4] H. Li, T.-T. Sun, S.-G. Zhang, J.-M. Shi. *J. Coord. Chem*., **63**, 1531 (2010).
[5] C. Wang, J. Li, Y.-W. Ren, F.-G. He, G. Meke, F.-X. Zhang. *J. Coord. Chem*., **61**, 4033 (2008).
[6] H. Li, C. Hou, J.-M. Shi, S.-G. Zhang. *J. Coord. Chem*., **61**, 3501 (2008).
[7] J.-M. Li, X. Jin. *J. Coord. Chem*., **62**, 2610 (2009).
[8] J.-M. Shi, Q.S. Liu, W. Shi. *J. Coord. Chem*., **62**, 1121 (2009).
[9] N.P. Gritsan, A.V. Lonchakov, E. Lork, R. Mews, E.A. Pritchina, A.V. Zibarev. *Eur. J. Inorg. Chem*., 1994 (2008).
[10] K. Goto, T. Kubo, K. Yamamoto, K. Nakasuji, K. Sato, D. Shiomi, T. Takui, M. Kubota, T. Kobayashi, K. Yakusi, J. Ouyang. *J. Am. Chem. Soc*., **121**, 1619 (1999).
[11] B.D. Koivisto, A.S. Ichimura, R. McDonald, M.T. Lemaire, L.K. Thompson, R.G. Hicks. *J. Am. Chem. Soc*., **128**, 690 (2006).
[12] J.A. Bertrand, T.D. Black, P.G. Eller, F.T. Helm, R. Mahmood. *Inorg. Chem*., **15**, 2965 (1976).
[13] D. Maspoch, L. Catala, P. Gerbier, D. Ruiz-Molina, J. Vidal-Gancedo, K. Wurst, C. Rovira, J. Veciana. *Chem. Eur. J*., **8**, 3635 (2002).
[14] J.L. Manson, J.A. Schlueter, K.A. Funk, H.I. Southerland, B. Twamley, T. Lancaster, S.J. Blundell, P.J. Baker, F.L. Pratt, J. Singleton, R.D. McDonald, P.A. Goddard, P. Sengupta, C.D. Batista, L. Ding, C. Lee, M.-H. Whangbo, I. Franke, S. Cox, C. Baines, D. Tria. *J. Am. Chem. Soc*., **131**, 6733 (2009).
[15] J. Tang, J.S. Costa, A. Golobic, B. Kozlevcar, A. Robertazzi, A.V. Vargiu, P. Gamez, J. Reedijk. *Inorg. Chem*., **48**, 5473 (2009).
[16] B. Sarkar, S. Konar, C.J. Gomez-Garcıa, A. Ghosh. *Inorg. Chem*., **47**, 11611 (2008).
[17] M.S. Ray, A. Ghosh, R. Bhattacharya, G. Mukhopadhyay, M.G.B. Drew, J. Ribas. *Dalton Trans*., 252 (2004).
[18] M.S. Ray, A. Ghosh, S. Chaudhuri, M.G.B. Drew, J. Ribas. *Eur. J. Inorg. Chem*., 3110 (2004).
[19] W.-Z. Shen, X.-Y. Chen, P. Cheng, S.-P. Yan, B. Zhai, D.-Z. Liao, Z.-H. Jiang. *Eur. J. Inorg. Chem*., 2297 (2005).
[20] C. Rancurel, N. Daro, O.B. Borobia, E. Herdtweck, J.-P. Sutter. *Eur. J. Org. Chem*., 167 (2003).
[21] C. Faulmann, E. Riviere, S. Dorbes, F. Senocq, E. Coronado, P. Cassoux. *Eur. J. Inorg. Chem*., 2880 (2003).
[22] L. Norel, F. Pointillart, C. Train, L.-M. Chamoreau, K. Boubekeur, Y. Journaux, A. Brieger, D.J.R. Brook. *Inorg. Chem*., **47**, 2396 (2008).
[23] X.M. Ren, S. Nishihara, T. Akutagawa, S. Noro, T. Nakamura. *Inorg. Chem*., **45**, 2229 (2006).
[24] S.G. Zhang, L.-M. Xie. *Acta Crystallogr*., **E65**, m1235 (2009).
[25] L. Noodleman. *J. Chem. Phys*., **74**, 5737 (1981).
[26] L. Noodleman, E.J. Baerends. *J. Am. Chem. Soc*., **106**, 2316 (1984).
[27] L. Noodleman, D.A. Case. *Adv. Inorg. Chem*., **38**, 423 (1992).
[28] F. Neese. An Ab Initio, DFT and Semiempirical Electronic Structure Package, Program Version 2.7, Revision 0; Lehrstuhl fuer Theoretische Chemie Institut fuer Physikalische und Theoretische Chemie, Universitaet Bonn, Germany, 20, Jan. (2010).
[29] A.D. Becke. *J. Chem. Phys*., **98**, 5648 (1993).
[30] A.D. Becke. *Phys. Rev. A*, **38**, 3098 (1988).
[31] C. Lee, W. Yang, R.G. Parr. *Phys. Rev. B*, **37**, 785 (1988).
[32] J. Cano, E. Ruiz, S. Alvarez, M. Verdaguer. *Comments Inorg. Chem*., **20**, 27 (1998).
[33] E. Ruiz, P. Alemany, S. Alvarez, J. Cano. *J. Am. Chem. Soc*., **119**, 1297 (1997).
[34] A. Schaefer, H. Horn, R. Ahlrichs. *J. Chem. Phys*., **97**, 2571 (1992).
[35] F. Weigend, R. Ahlrichs. *Phys. Chem. Chem. Phys*., **7**, 3297 (2005).
[36] A.W. Addison, T.N. Rao, J. Reedjik, J. van Rijn, C.G. Verschoor. *J. Chem. Soc., Dalton Trans*., 1349 (1984).
[37] C. Janiak. *J. Chem. Soc., Dalton Trans*., 3885 (2000).
[38] Y. Rodriguez-Martin, J. Sanchiz, C. Ruiz-Perez, F. Lloretc, M. Julve. *Cryst. Eng. Commun*., **4**, 631 (2002).
[39] P. Baran, R. Boca, M. Breza, H. Elias, H. Fuess, V. Jorik, R. Klement, I. Svoboda. *Polyhedron*, **21**, 1561 (2002).
[40] S. Salunke-Gawali, S.Y. Rane, V.G. Puranik, C. Guyard-Duhayon, F. Varret. *Polyhedron*, **23**, 2541 (2004).
[41] P. Talukder, S. Sen, S. Mitra, L. Dahlenberg, C. Desplanches, J.-P. Sutter. *Eur. J. Inorg. Chem*., 329 (2006).

[42] N. Arulsamy, J. Glerup, D.J. Hodgson. *Inorg. Chem.*, **33**, 2066 (1994).
[43] K. Yoshizawa, R. Hoffmann. *J. Am. Chem. Soc.*, **117**, 6921 (1995).
[44] C. Faulmann, E. Riviere, S. Dorbes, F. Senocq, E. Coronado, P. Cassoux. *Eur. J. Inorg. Chem.*, 2880 (2003).
[45] O. Kahn. *Molecular Magnetism*, VCH, New York (1993).